OPTICAL FILTERS

An optical filter is any device or material which is used to change the spectral composition of an incoming electromagnetic field. Optical filters are used to modify both the spectral power and the phase distributions.

Optical filters operate in the visible, ultraviolet and near infrared wavelength regions. Depending on the application, their spectral behavior is described in terms of the wavelength λ, the frequency ω or the wave number $k_0 = 2\pi/\lambda$ of the electromagnetic field in vacuum.

We will first define the basic filter parameters and measurement techniques. A discussion of the most important filter concepts then forms the central part of this article, whereas acoustooptical devices and spectrometers are treated elsewhere in the encyclopedia. The applications of optical filters in optical communication systems, sensors, consumer products, lasers and other optical instruments are briefly sketched.

Transfer matrix theories (see section entitled "Co- and Contradirectional Couplers") or the equivalent characteristic matrices (see section entitled "Interference Filters") are increasingly preferred as a means of describing optical filters, since they offer a straightforward way of calculating stacked filters and even more complex circuitries.

BASIC EQUATIONS AND PARAMETERS

The majority of optical filters are linear devices, i.e., the spectral response $\Phi_o(\omega)$ of an optical filter to an incoming signal $\Phi_i(\omega)$ is given by

$$\Phi_o(\omega) = H(\omega)\Phi_i(\omega) \tag{1}$$

where $H(\omega)$ stands for the transfer function of the optical filter. Within this article, a forward traveling wave is described by $\Phi = \exp(j(\mathbf{kr} - \omega t))$ with the position vector $\mathbf{r}$ and the time t. Some signs in phase-sensitive expressions will be affected by this basic assumption.

Today, most optical filters are used in phase-insensitive assemblies. For such applications, the optical filter is completely described by its response to an incoming optical power distribution $Pi(\omega) \propto |\Phi_i(\omega)|^2$, i.e.,

$$P_o(\omega) = |H(\omega)|^2 P_i(\omega) \tag{2}$$

Figure 1 serves as an illustration for the following discussion of the most important filter parameters.

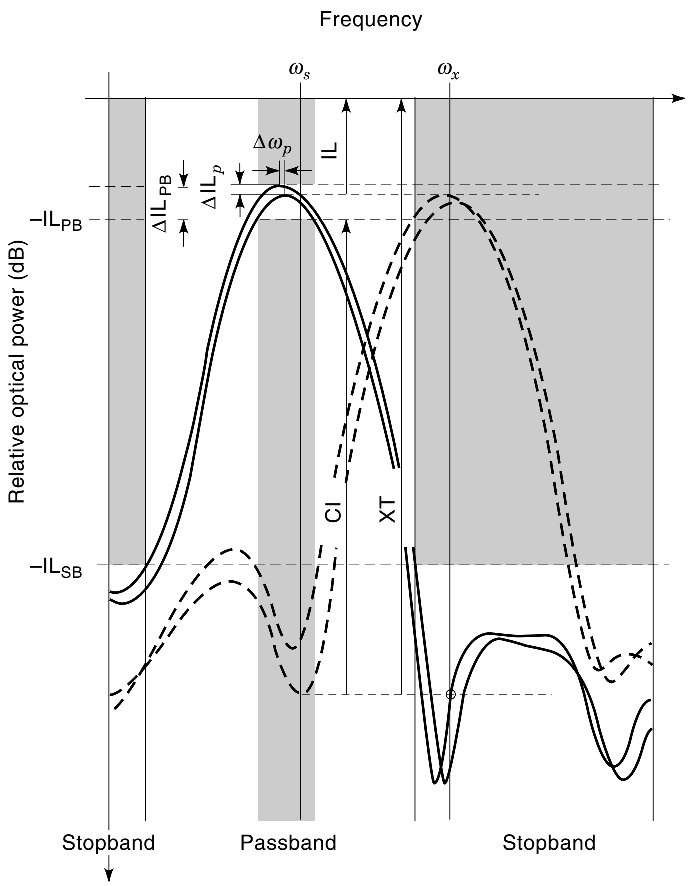

Figure 1. Relevant parameters of optical filters (IL: insertion loss, XT: crosstalk attenuation, CI: channel isolation, $\mathrm{IL}_{\mathrm{PB}}$, $\mathrm{IL}_{\mathrm{SB}}$: maximum/minimum insertion loss in the passband/stopband, $\Delta\mathrm{IL}_p/\Delta\omega_p$: additional insertion loss/equivalent frequency shift due to polarization), ω_s, ω_x: signal and crosstalk frequencies).

Insertion Loss

The insertion loss of an arbitrary optical device is the fraction of optical power which is lost by moving the device into the optical path. The insertion loss of an optical filter at a signal frequency ω_s is defined by

$$\mathrm{IL}(\omega_s) = 10 \cdot \log_{10} |H(\omega_s)|^2 \tag{3}$$

It should be noted that the insertion loss is defined via the ratio of the optical powers of incoming and outgoing signals, and not via the corresponding electrical power levels within the detection circuitry.

Crosstalk Attenuation/Channel Isolation

For a set of closely spaced transmission lines, crosstalk is defined as the relative power transfer to a nonexcited line. Analogously, the crosstalk attenuation XT of an optical filter is defined as the insertion loss in another channel at a frequency ω_x, that is,

$$\mathrm{XT}(\omega_x) = \mathrm{IL}(\omega_x) \tag{4}$$

Any treatment of crosstalk at a signal frequency ($\omega_x = \omega_s$) which is typical for echoes or reallocated frequency channels must take coherent effects into account. The channel isolation

$$\mathrm{CI}(\omega_x) = \mathrm{XT}(\omega_x) - \mathrm{IL}_{\mathrm{PB}} \tag{5}$$

relates the crosstalk attenuation to a reference insertion loss $\mathrm{IL}_{\mathrm{PB}}$, usually the maximum insertion loss within a passband. It should be noted that the accumulated crosstalk from many spectrally distant sources of a multichannel system can become significantly higher than that of the two adjacent channels. By cascading optical filters it is always possible to improve the crosstalk attenuation at the expense of a reduced filter bandwidth.

Passband/Stopband

A passband $[\omega_{\min}^{(\mathrm{PB})}, \omega_{\max}^{(\mathrm{PB})}]$ of an optical filter is a frequency interval offering "low" insertion losses, that is,

$$\mathrm{IL}_{\mathrm{PB}} \geq \mathrm{IL}(\omega_{\min}^{(\mathrm{PB})} \leq \omega \leq \omega_{\max}^{(\mathrm{PB})}) \geq \mathrm{IL}_{\mathrm{PB}} - \Delta\mathrm{IL}_{\mathrm{PB}} \tag{6}$$

$\mathrm{IL}_{\mathrm{PB}}$ is the maximum insertion loss tolerated in the passband. Ranges of acceptable insertion losses are typically $\Delta\mathrm{IL}_{\mathrm{PB}} = 1 \ldots 3$ dB depending on the number of cascaded filters. A stopband $[\omega_{\min}^{(\mathrm{SB})}, \omega_{\max}^{(\mathrm{SB})}]$ of an optical filter, in contrast, is a frequency range offering "high" insertion losses,

$$\mathrm{IL}(\omega_{\min}^{(\mathrm{SB})} \leq \omega \leq \omega_{\max}^{(\mathrm{SB})}) \geq \mathrm{IL}_{\mathrm{SB}} \tag{7}$$

where $\mathrm{IL}_{\mathrm{SB}}$ stands for the minimum insertion loss in the stopband.

The roll-off of an optical filter is given by the slope of the filter curve. It determines the extent of the spectral range between the passband and the stopband which cannot be used for most applications.

Group Delay/Dispersion

The group delay

$$t_g(\omega_s) = -\left.\frac{\partial\varphi}{\partial\omega}\right|_{\omega_s} \tag{8}$$

caused by an optical filter at a signal frequency ω_s is given by the first derivative $d\varphi/d\omega$ of the phase of the transfer function $H(\omega_s) = |H(\omega_s)| \exp(j\varphi(\omega_s))$.

The group velocity dispersion (GVD)

$$\mathrm{GVD}(\omega_s) = \frac{\partial t_g}{\partial\lambda} = \left.\frac{\omega_s^2}{2\pi c}\frac{\partial^2\varphi}{\partial\omega^2}\right|_{\omega_s} \tag{9}$$

is defined as the additional group delay per wavelength deviation. The definitions of the group delay t_g and the GVD can be verified by studying the propagation of a Gaussian pulse through a purely phase-distorting optical filter.

The GVD leads to compression and decompression of optical pulses as well as to a linear chirp.

Polarization Dependent Parameters

Most optical filters are more or less polarization sensitive devices, that is, the insertion loss measured at a certain frequency varies according to the polarization state of the input signal. Over an extended spectral region, the ranges of possible insertion losses form a band which allows the polarization dependent behavior of an optical filter to be assessed. For the majority of devices, the boundaries of these bands are given by two orthogonal polarization states (s- and p-polarization for interference filters, TE- and TM-polarization for integrated optical devices) irrespective of the wavelength.

The design of filters usually aims to minimize the polarization sensitivity. For many filters of this type, the boundaries of the bands of possible insertion losses are represented by two filter curves of almost the same shape (see Fig. 1) which are shifted with respect to each other. The residual polarization dependence can then be described by an equivalent frequency shift $\Delta\omega_p$ and an additional insertion loss $\Delta\mathrm{IL}_p$ for one of the polarization states.

Spectral Resolution/Free Spectral Range

According to the generalized Rayleigh's criterion, the spectral resolution $\Delta\omega_{\mathrm{RC}}$ of an optical filter is given by the full width half maximum (FWHM) of its filter curve. The transfer function of a filter which is periodic with respect to the frequency or wave number satisfies the condition

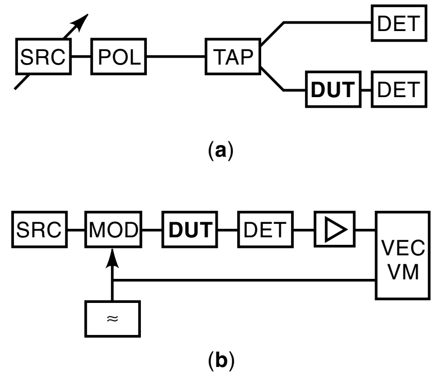

Figure 2. Measurement setups for insertion loss (a) and group delay (b) (DUT: device under test, SRC: optical source, $\approx$: microwave source, POL: polarizer, MOD: amplitude modulator, TAP: optical tap (1 : 10), DET: detector, VEC–VM: vector voltmeter, $\triangleright$: amplifier).

$$H(\omega + \Delta\omega_{\mathrm{FSR}}) = H(\omega) \tag{10}$$

The period $\Delta\omega_{\mathrm{FSR}}$ designates the free spectral range of the optical filter, i.e., the spectral range of nonoverlapping operation. The maximum number $N_{\max}$ of channels, which can be separated by a periodic filter (e.g., a Fabry–Perot interferometer) according to Rayleigh's criterion is given by $N_{\max} = \Delta\omega_{\mathrm{FSR}}/\Delta\omega_{\mathrm{RC}}$. The true number of frequency channels depends on the crosstalk requirements of the underlying application.

Measurement Setups

The spectral characterization of optical filters concentrates on two different parameters: insertion loss and group delay.

Figure 2(a) shows a typical setup for the measurement of the insertion loss. The light transmitted through the optical filter is emitted from a tunable source which is built up as a tunable laser (e.g., an external cavity laser) or as a broadband source [e.g., a light emitting diode (LED) or a white light source] combined with a monochromator. The beam is then transmitted through a polarizer before a small part of the optical power is split off as a reference signal. The signal is subsequently transmitted through the optical filter. Signal and reference are detected by two optical power meters. Lock-in techniques are used to improve the accuracy.

Figure 2(b) shows a setup for the measurement of the group delay of an optical filter. It measures the group delay of a microwave signal directly. The light transmitted through the optical filter is again emitted from a tunable source. The beam is then transmitted through a modulator where the amplitude of the optical beam is modulated by the microwave signal. The signal is finally detected and amplified in the electrical domain before being compared with the reference microwave signal by using a vector voltmeter or a network analyzer. The resolution of the setup increases in accordance with the increasing frequency of the microwave signal. The amplitude modulator, the direct detection receiver as well as the vector voltmeter therefore need to be high-speed devices.

SYSTEMS WITH OPTICAL FILTERS

The optical circuitry required for the transmission or detection of several frequency channels can be laid out in four different ways (see Fig. 3). The first concept (spectrograph) separates all the frequency channels in one step. It represents the best solution for the parallel processing of many channels. The required multichannel filters are reflection or transmission gratings, prisms or optical phased arrays. The second concept (chain) consists of a cascade of filters. Each filter (typically an interference filter) along the chain adds or drops one frequency channel. It represents a modular solution for ADD/DROP applications. The accumulation of insertion losses along the chain results in declining the power levels of the different frequency channels. The third concept (array) consists of an array of filters which are connected in parallel. Each filter (typically a Fabry–Perot interferometer) represents a band-pass for one of the frequency channels. This concept suffers from an inherent splitting loss ($IL_s = 10 \log N$). The fourth concept (tree) is based on a binary tree, usually of periodic filters. Each filter (typically a directional or Mach–Zehnder coupler or interference filter) routes every second frequency channel or the upper or lower half of the frequency channels to one output port, that is, each filter must be adapted to the underlying system.

During the last few years, the range of applications has shifted from classical sectors, mainly spectroscopy and lasers, to optical communication systems and sensors. In consequence increasing numbers of optical filters are now equipped with fiber pigtails. Microoptical and integrated optical devices are increasingly ousting out their classical equivalents.

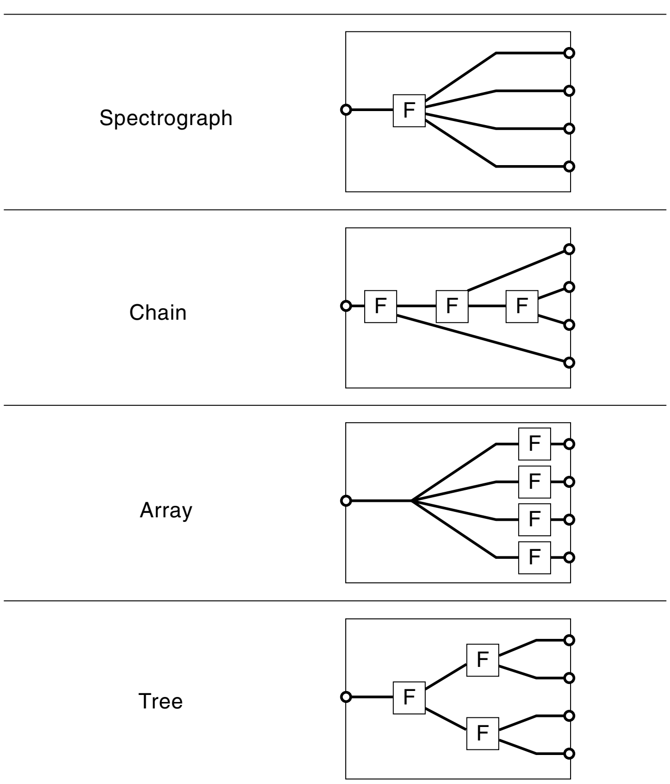

Figure 3. Basic optical filter circuitries (Spectrograph, Chain, Array, Tree).

Spectroscopy

Spectrometers and spectrographs are the classical instruments used in spectroscopy. Spectrometers are tunable filters which can sweep over the optical spectrum. They are often used as monochromators. Spectrographs, in contrast to spectrometers, allow parallel processing of the optical spectrum. A great variety of mountings is available each of which is optimized with respect to the underlying application. A large free spectral range and a high spectral resolution are the key parameters of spectrometers and spectrographs. For this reason, reflection gratings operated in the first-order of diffraction form the core of most of these instruments. For deep-UV applications, special prisms serve as optical filters. Additional broadband filters (usually interference filters) are often placed in front of spectrometers and spectrographs in order to restrict the spectrum to one order of diffraction.

Spectrometers and spectrographs are typical representatives of laboratory equipment. Most of these devices are bulky and should be operated in a laboratory environment.

Communications Systems

Optical filters play an increasing role in optical communications systems.

Today, the worldwide telecommunications core network is based mainly on single-mode fibers. The transmission systems are operated in the near infrared wavelength region ($1.3\ \mu m \ldots 1.5\ \mu m$) where both the attenuation and the GVD of the optical fibers are small. The remaining limitations of optical transmission due to fiber loss and dispersion have been overcome by introducing erbium-doped fiber amplifiers (EDFAs) and dispersion management. The maximum transmission length of today's high bitrate systems is power dependent. It is limited at the low power side by noise accumulation and at the high power side by fiber nonlinearities. Most long-haul transmission lines (>150 km) have been equipped with EDFAs resulting in a substantially reduced number of electrical 3R-repeaters. Optical filters (mainly fiber based directional couplers, Mach–Zehnder devices, and interference filters) are used to flatten their gain characteristics. Tunable filters are used to restrict the spectrum of the amplified spontaneous emission (ASE) and thus the ASE–ASE beat noise occurring at the receiver. With an increasing data rate the compensation of fiber dispersion becomes increasingly important. In addition to dispersion compensating fibers, optical filters (mainly chirped Bragg gratings) can be used to compensate the group velocity dispersion of the fibers.

An increasing number of transmission lines is operated in wavelength division multiplex (WDM) mode in order to upgrade the capacity of existing fibers. According to the standards of the International Telecommunications Union (ITU), the WDM channels are located in the amplification band of the EDFA around $1.55\ \mu m$. The spacing of these channels is given by multiples of 100 GHz (≈ 0.8 nm at $1.5\ \mu m$). Optical filters are used as wavelength demultiplexers and, for systems with many wavelength channels, also as wavelength multiplexers. They are critical high-end components in the layout of such systems. The corresponding components are realized as spectrographs (optical phased arrays or reflection gratings), chains of optical filters (usually interference filters) or an array of passband filters (fiber Bragg gratings or Fabry–Perot filters). Wavelength division multiplex represents a high-end application for optical filters. The required channel isolation (typically >20 dB for adjacent wavelength channels and >30 dB for distant wavelength channels) for an arbitrary polarization state represents the central requirement for transmission systems with many WDM channels. The tolerated insertion loss is determined by the layout of the system. It represents a critical quantity for WDM links without optical amplifiers (typical specification: 5 dB). The core network is moving toward an all-optical network which is characterized by reconfigurable links in the optical domain on the basis of WDM transmission. Key components of such networks are optical add-drop multiplexers (OADM) and optical cross connects (OXC). OADMs allow one or more WDM channels to be added to and/or dropped from a WDM transmission system. The core of such a component is formed by one or more tunable filters or by a wavelength multiplexer/demultiplexer pair separated by a passive circuitry. An OXC consists a multiplexer and a demultiplexer separated by a switching matrix. It allows wavelength channels to be exchanged between different fibers. If wavelength converters are additionally installed, the OXC can switch wavelength channels in the same way as fiber channels. OADMs are currently entering the market, while OXCs are being tested in field trials.

Optical fibers are currently also moving into the access networks. Fiber to the curb (FTTC) systems, which are based on bidirectional full-duplex transmission, use optical filters (mainly interference filters) to separate the two wavelengths used for upstream and downstream transmission. These transmission lines use a wide channel spacing (today usually >200 nm) to allow high wavelength tolerances for the lasers. From the point of view of the optical filter, the required isolation of the counter propagating signals with greatly differing power levels (typically >50 dB for the complete setup) and the low price are the critical parameters for this component. Optical filters used for such systems are interference filters and directional couplers (fiber-based and integrated optical solutions).

Optical communications systems require robust and compact components which can be used in the field under tough environmental conditions. For this reason most of the optical components are manufactured by using the technologies of microoptics or integrated optics.

Sensors

Sensors form part of most systems today and will play an increasing role in view of the growing possibilities offered by signal processing. Photonics can be used within sensor systems for detection, communications, and power supply applications. Competitive advantages of optical communications and power supply systems include: no electromagnetic interference, electrical isolation, and high explosion safety. The photonic sensors themselves can be divided into two classes: true photonic sensors and photon-assisted sensors.

True photonic sensors detect and/or analyze optical signals. Examples of this type of sensing are absorption analysis and spectroscopy. Beside the classical laboratory spectrometers and spectrographs, there is an increasing field of application for microoptical devices. An example is given by the integrated optical spectrographs which are used to calibrate high-end printers by measuring their color temperature.

Photon-assisted sensors detect the influence of an acoustic, electrical or chemical signal on the behavior of an optical wave. Some of these sensors are based on the detuning of optical filters, mainly of Mach–Zehnder or Michelson interferometers. Examples of this kind are gyroscopes, position sensors, and vapor sensors (e.g., SO_2 and NH_3). Strain sensors based on detuned fiber Bragg gratings have also been implemented.

Photonic sensors find application in industrial and military environments (e.g., chemical plants, oil platforms), transportation (e.g., aircraft), electrical power plants and distribution systems, as well as robotics and machine-control systems. Although the cost of photonic equipment has dropped dramatically, high costs still often prevent more extensive use of these sensors.

Other Applications

Anti-reflection (AR) coatings and mirrors are the most important applications which have not yet been covered. AR coatings are used for dereflecting lenses and other optical interfaces inside optical instruments, lasers, and laboratory equipment, but also in typical consumer products such as spectacles and camera lenses. Interference filters are also used as mirrors in resonators for lasers and Fabry–Perot interferometers. Beam splitters, neutral filters, and similar devices form further applications.

INTERFERENCE FILTERS AND FABRY–PEROT INTERFEROMETERS

Fabry–Perot interferometers and interference filters are based on the interference of electromagnetic radiation in a series of plane–parallel (usually dielectric) interfaces.

Reflection and Refraction

The directions of propagation of the reflected and the transmitted waves passing through a planar dielectric interface between two media i and o with refractive indices n_i and n_o respectively, can easily be determined by the law of reflection $\theta_r = \theta_i$ and Snell's law of refraction $n_o \sin\theta_o = n_i \sin\theta_i$.

Fresnel's formulas are used to calculate the reflection coefficient

$$r = \frac{\eta_i - \eta_o}{\eta_i + \eta_o} \tag{11}$$

and the transmission coefficient

$$t = \frac{2\eta_i}{\eta_i + \eta_o} \tag{12}$$

The characteristic admittance η

$$\eta = \begin{cases} \sqrt{n^2 - n_i^2 \sin^2\theta_i} & \text{for } s\text{-polarization} \\ n^2/\sqrt{n^2 - n_i^2 \sin^2\theta_i} & \text{for } p\text{-polarization} \end{cases} \tag{13}$$

allows a unified treatment of s- and p-polarization. For s-polarization, the electric field is perpendicular to the plane of incidence, whereas for p-polarization it is parallel to it.

The reflectance, that is, the relative reflected power, is given by $R = |r|^2$. The transmittance, that is, the relative transmitted power is determined by $T = |t|^2\mathrm{Re}(\eta_o)/\mathrm{Re}(\eta_i)$.

The effect of passing a plane–parallel plate of thickness d and refractive index n is described by using the equivalent phase thickness

$$\delta = k_0 d\sqrt{n^2 - n_i^2 \sin^2\theta_i} \tag{14}$$

of the layer. For transparent media and angles below the critical angle of total reflection, the coefficient $e^{i\delta}$ will be a pure phase factor, whereas lossy material will be subject to an attenuation of $|e^{i\delta}| < 1$.

Fabry–Perot Interferometer

The Fabry–Perot interferometer is formed by a single cavity embedded between two plane–parallel, nearly perfect mirrors. Its reflection coefficient is given by

$$r_{\mathrm{FP}} = \frac{r_i + r_o e^{2i\delta}}{1 + r_i r_o e^{2i\delta}} \tag{15}$$

where r_i and r_o stand for the reflection coefficients at the input and output interfaces, respectively. The expression for the reflection coefficient of the Fabry–Perot interferometer is usually derived by summing the amplitudes of all partial reflections and refractions (Airy's summation). It can also be calculated by using the characteristic matrices introduced in the section entitled "Interference Filters."

For symmetric arrangements, $r = -r_i = r_o$, lossless media and angles below the critical angle of total reflection ($|e^{i\delta}| = 1$, $\phi_r = 0$), the reflectance is given by

$$R_{\mathrm{FP}} = \frac{F^2 \sin^2\delta}{(\pi/2)^2 + F^2\sin^2\delta} \tag{16}$$

where

$$F = \frac{\pi\sqrt{R}}{1-R} \tag{17}$$

designates the finesse of the Fabry–Perot interferometer (1). Figure 4 shows filter curves for this case. No reflection occurs if the condition $\delta = m\pi$ is satisfied. The free spectral range is given by $\Delta\delta_{\mathrm{FSR}} = \pi$, that is,

$$\Delta\lambda_{\mathrm{FSR}} = \frac{\lambda^2}{2d\sqrt{n^2 - n_i^2\sin^2\theta_i}} \tag{18}$$

The FWHM of the filter is

$$\Delta\delta_{\mathrm{FWHM}} = 2\sin^{-1}\left(\frac{\pi}{2F}\right) \approx \frac{\Delta\delta_{\mathrm{FSR}}}{F} \tag{19}$$

Equation (19) shows that the finesse represents the number of wavelength channels which can be placed within one free spectral range when the channel spacing coincides with the full width half maximum. The transmittance does not vanish completely even in the regime of total reflection. Its minimum value is given by

$$T_{\mathrm{FP}}^{(\mathrm{min})} = \frac{(\pi/2)^2}{(\pi/2)^2 + F^2} \approx \left(\frac{\pi}{2F}\right)^2 \tag{20}$$

This phenomenon is called tunneling in conformity with the terminology of quantum mechanics (2).

Today, Fabry–Perot interferometers are mainly used as tunable band-pass filters. Interference filters act as the highly reflecting mirrors forming the resonator. The finesse of these interferometers is limited by imperfections of the resonator especially in tunable filters and by diffraction inside the resonator. Fabry–Perot interferometers are usually tuned by moving one of the mirrors. Devices whose cavities are filled with liquid crystals can be tuned without moving the mirrors, but they suffer from polarization dependence and additional insertion losses caused by the liquid crystal. Fabry–Perot interferometers with finesses of up to several hundred are available on the market. Their disadvantages are a low tuning speed and a frequently occurring hysteresis of the tuning curve.

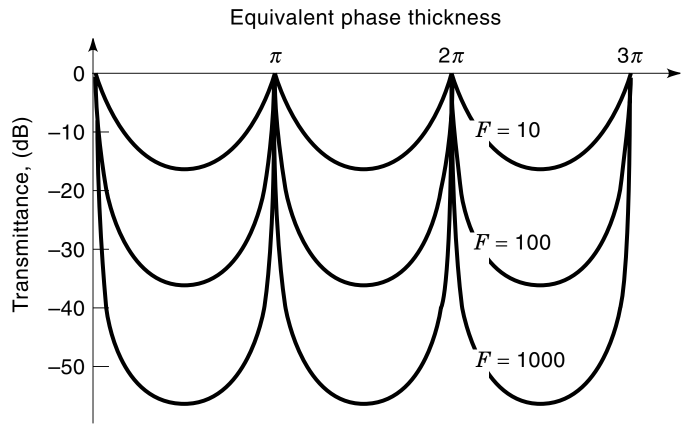

Figure 4. Filter curves versus equivalent phase thickness of Fabry–Perot interferometers with various finesses (F = 10, 100, 1000).

Interference Filters

Interference filters consist of a series of thin films which can be deposited by evaporation, ion-assisted deposition, ion plating, sputtering or even by various epitaxial processes. Interference filters can also be deposited from the liquid phase, but this technique is declining in importance due to the increase in fabrication tolerances. The choice of coating materials and fabrication process is driven by the type of filter and by the environmental specifications, especially the degree of hardness and the resistance to humidity. An extensive list of available coating materials is presented in the textbook by Macleod (3).

Characteristic Matrix. Using the fundamental solutions of Maxwell's equations in a homogeneous space, which take both forward and backward traveling waves into account, the propagation of the electromagnetic field is given by

$$\begin{pmatrix} E_i \\ jH_i \end{pmatrix} = \mathscr{U} \begin{pmatrix} E_o \\ jH_o \end{pmatrix} \tag{21}$$

The characteristic matrix $\mathscr{U}$ with the elements u_{ij} describes the transfer of the optical field through a single homogeneous layer of thickness d and refractive index n. It is given by

$$\mathscr{U} = \begin{pmatrix} \cos\delta & -\sin\delta/\eta \\ \eta\sin\delta & \cos\delta \end{pmatrix} \tag{22}$$

with the characteristic admittance η and the phase thickness δ of the layer. Since the tangential components of both the electric and the magnetic field are continuous at a dielectric interface, an arbitrary interference filter consisting of L layers can be described by stacking up the characteristic matrices, i.e., $\mathscr{U} = \prod_{l=1}^{L}\mathscr{U}_l = \mathscr{U}_1\mathscr{U}_2 \ldots \mathscr{U}_L$. The admittance Y of the interference filter is given by

$$jY = \frac{u_{21} + ju_{22}\eta_o}{u_{11} + ju_{12}\eta_o} \tag{23}$$

where η_i and η_o stand for the admittances of the input and output media. Matching the tangential field components at the first dielectric interface of the interference filter yields the following relation for the reflection coefficient:

$$r_{\mathrm{IF}} = \frac{\eta_i - Y}{\eta_i + Y} \tag{24}$$

Equation (12) for the transmission coefficient and the equations for reflectance and transmittance at a single interface can be applied to interference filters simply by replacing the admittance of the output medium η_o by that of the interference filter.

Lossless Filters. The lossless interference filters characterized by a real refractive index n form the most important class of interference filters. They are described by unimodular 2×2-matrices (see the Appendix for some of their properties).

For particular wavelengths, where the optical thickness is an integral number of quarter-waves, the characteristic matrix is given by

$$\mathscr{U} = \begin{cases} (-1)^{N/2}\begin{pmatrix} 1 & 0 \\ 0 & 1 \end{pmatrix} & \text{for even } N \\ (-1)^{(N+1)/2}\begin{pmatrix} 0 & 1/\eta_j \\ -\eta_j & 0 \end{pmatrix} & \text{for odd } N \end{cases} \tag{25}$$

i.e., half-wave layers are optically transparent. A convenient notation is obtained by defining the interference filters at a design wavelength in terms of quarter-wave layers. The characters H, L, and M usually refer to quarter-wave layers of high, low, and intermediate refractive index, respectively.

The characteristic matrix of an N-period multilayer can be calculated by using Chebyshev polynominals. Spectral regions with $|\mathrm{Tr}\mathscr{U}| > 2$ are designated as its (potential) stopbands since an infinite periodic stack of multilayers ($N \to \infty$) acts as a perfect reflector ($R = 1$) within these bands. The widths of the stopbands represent a measure of the refractive index contrast of the basic period. With decreasing refractive index contrast, the width of a stopband tends to zero. A necessary condition for the occurrence of a stopband at the wavelength λ_l is therefore

$$\frac{2\pi}{\lambda_l}\sqrt{n^2 - n_i^2\sin^2\theta_i} = \frac{l\pi}{\Lambda} \tag{26}$$

in which Λ is the period, that is, the thickness of the basic period. However, if any of the layers forming the basic period is transparent for a certain order l, the stopband cannot be observed. The stack $(HL)^N$, for example, has no even orders for that reason. This equation is in fact the Bragg condition that governs any type of contradirectional coupler.

A symmetric stack of layers $\mathscr{U} = \mathscr{U}_1\mathscr{U}_2 \ldots \mathscr{U}_L \ldots \mathscr{U}_2\mathscr{U}_1$ can be replaced by a single equivalent layer with the characteristic matrix

$$\mathscr{U} = \begin{pmatrix} \cos\Delta & \sin\Delta/H \\ -H\sin\Delta & \cos\Delta \end{pmatrix} \tag{27}$$

The equivalent phase thickness Δ is given by $\cos\Delta = u_{11}$. It is either purely real or purely imaginary. The equivalent admittance η_{eq} is defined by $\eta_{\mathrm{eq}} = \sqrt{-u_{21}/u_{12}}$.

Examples. Figure 5 shows a simple design and a schematic diagram of the filter curve for the four most important types of interference filter—anti-reflection coating, low-pass, high-pass, and band-pass filters. It should be pointed out that the edge filters—low-pass and high-pass types—should be operated at their fundamental order since the behavior of the filter curve close to the stopband changes at higher orders. More sophisticated designs can be obtained by refining the filter curves of such simple designs, that is, by varying the thickness of certain layers to reduce the ripples of the filter curve in its passband. A more detailed discussion of this topic is given in (3–5).

CO- AND CONTRADIRECTIONAL COUPLERS

Co- and contradirectional couplers are any devices based on the coupling of guided modes. A small selection of these devices will be examined in the following.

Transfer Matrix Theory

Transfer matrix theory represents a common theory which provides a description of any circuitry built up from co- and contradirectional couplers. The transfer matrix for a general coupler with N interacting modes is given by a $N \times N$ matrix. It describes the transfer of modes through the coupling structure.

For a purely passive coupler, the sum of the reflected and transmitted powers at all ports is always smaller than or equal to the incoming power. The losses are caused by radiation and absorption. Theoretical descriptions for both lossless

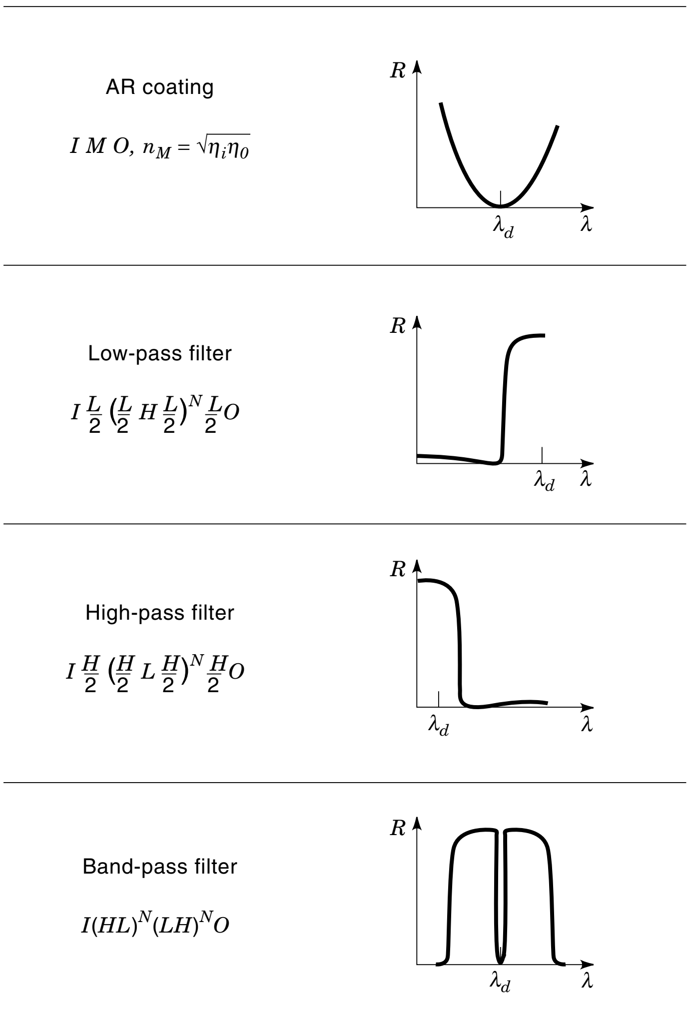

Figure 5. Basic types of interference filter (AR coating, low-pass filter, high-pass filter, band-pass filter). H, L, and M refer to quarter-wave layers of high, low, and intermediate refractive index, and I and O refer to the input and output media.

and lossy devices are available. However, most coupler structures can be treated approximately as lossless devices. Such devices are modeled by unimodular matrices.

Two Interacting Modes. For the most important case of two interacting modes the transfer matrix of a lossless device is given by

$$\mathscr{U}_\pm = \begin{pmatrix} A^\ominus & A^\otimes \\ \mp A^{\otimes *} & A^{\ominus *} \end{pmatrix} \tag{28}$$

where the upper sign applies to the codirectional case and the lower sign to the contradirectional one. Each type of transfer matrices ($\mathscr{U}_+$ and $\mathscr{U}_-$) forms a group, that is, the product of two transfer matrices results in a transfer matrix of the same type (see Appendix for some properties of the unimodular 2 × 2 matrix). The transfer matrix (for definitions of input and output ports, see Fig. 6)

$$\begin{pmatrix} a_1^{(o)} \\ a_2^{(o)} \end{pmatrix} = \mathscr{U}_\pm \begin{pmatrix} a_1^{(i)} \\ a_2^{(i)} \end{pmatrix} \tag{29}$$

describes the variation of the amplitudes a_i of the two modes propagating either co- or contradirectionally. The conservation of optical power is guaranteed by the relation

$$\left|a_1^{(o)}\right|^2 \pm \left|a_2^{(o)}\right|^2 = \left|a_1^{(i)}\right|^2 \pm \left|a_2^{(i)}\right|^2 \tag{30}$$

Cascaded couplers and couplers of varying cross section are described by the product of the transfer matrices of their constituents, that is, $\mathscr{U} = \prod_{l=1}^{L} \mathscr{U}_l = \mathscr{U}_1 \mathscr{U}_2 \ldots \mathscr{U}_L$. Sections of more complex networks are described by box-diagonal matrices (6).

Matrix Elements. There are several techniques for calculating the elements of a transfer matrix. The two most important are coupled mode theory (CMT) and the bidirectional eigenmode propagation method (BEP).

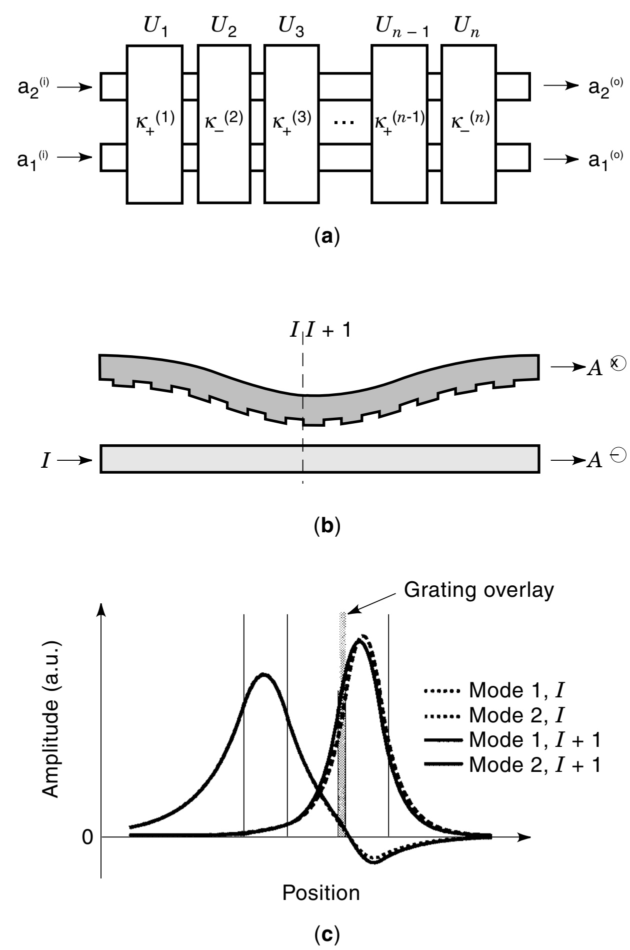

Figure 6. Periodically varying asymmetrical coupler: (a) representation by transfer matrices, (b) device structure composed of basic waveguide structures, (c) comparison of the field distributions on both sides of an abrupt change of the waveguide.

Coupled mode theory is a perturbation theory modeling a general coupler with N interacting modes. It starts from the coupled mode equations

$$-j\frac{\partial a_m}{\partial z} = k_m a_m + \sum_{l=1}^{N}(1-\delta_{ml})\kappa_{ml}a_l \tag{31}$$

where a_m and k_m describe the amplitude and wave number of the fundamental mode of a waveguide m, δ_{ml} stands for the Kronecker symbol. The coupling coefficients are given by its overlap integrals or Fourier coefficients. The elements of the transfer matrix in Eq. (28) calculated within the framework of coupled mode theory for the most elementary devices are given by

$$\begin{aligned} A^{\ominus}_{\pm} &= \cos(\delta_{\text{eff}}L) \pm j\delta\sin(\delta_{\text{eff}}L)/\delta_{\text{eff}} \\ A^{\otimes} &= j\kappa\sin(\delta_{\text{eff}}L)/\delta_{\text{eff}} \end{aligned} \tag{32}$$

in which $A^{\ominus}_{+}$ applies to the uniform directional coupler and $A^{\ominus}_{-}$ to the uniform Bragg grating. The definitions of the coupling coefficient κ, the detuning δ, and the effective detuning δ_{eff} are given in the sections entitled "Uniform Directional Couplers" and "Bragg Gratings."

The BEP method (7) is a powerful simulation tool which can be used to propagate an optical field under the influence of co- and contradirectional coupling. In a similar way to the beam propagation method (BPM), the BEP handles curved waveguides by means of stepwise changes. Within guided eigenmode propagation method [GEP Method (7)] the optical field is expanded into the eigenmodes of the coupled waveguide structure which then propagate undisturbed with their effective wave numbers k_i along sections with a constant refractive index profile. At any interface the eigenmodes are decomposed into the tangential components of the electric and magnetic fields which are then matched calculating the overlap integrals a_{ik} between the field distributions. The field distributions $E_i^{(l)}$ and $E_i^{(l+1)}$ of the eigenmodes i are slightly different in both sections (l and $l+1$), as sketched in Figs. 6(b) and 6(c). Each abrupt change of the waveguide structure leads to a mode conversion in which power is coupled from one mode to the other (or from one waveguide to the other). These transfer matrices coincide with those of coupled mode theory (7) for the weak coupling limit. Radiation modes can be neglected for the sake of simplicity, although the degree of the approximation is known at each step. The relevant expansion coefficients for codirectional devices are the overlap integrals between the even and odd eigenfunctions in both sections.

$$\begin{aligned} a_{ik}(\lambda) &= \int E_i^{(l+1)}(x)E_k^{(l)}(x)\,dx \\ \int E_i^l(x)E_k^l(x)\,dx &= \delta_{ik} \end{aligned} \tag{33}$$

The eigenmode calculation can be performed using either one-dimensional (calculated by the field transfer matrix method (8) or two-dimensional [calculated by the finite difference (FD) method] field distributions. The latter method involves greater numerical effort. In many cases a one-dimensional approach is accurate enough. It has the advantage of providing a numerical solution of an exactly solved equation. With today's personal computer power, this numerical process is very fast and accurate.

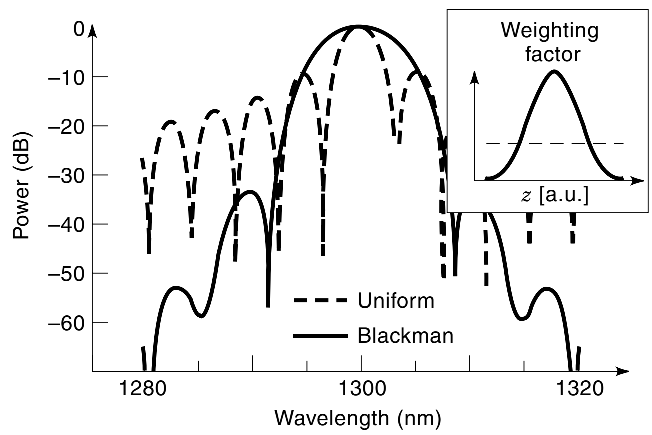

Figure 7. Filter curves for uniform (untapered) and κ-tapered devives showing the substantially reduced side-lobes for the Blackman window. The insert shows the corresponding weighting function, i.e., the mean coupling coefficient along the filter.

Side-Lobe Suppression. The side-lobes of co- and contradirectional couplers can be suppressed by appropriate tapering of the coupling coefficients, that is, by adiabatic variation of the coupling coefficient along the coupler. It can be shown (9,10) that the envelope of the filter curve is given by the Fourier transform of the tapered coupling coefficient. This makes the classical window functions used for digital filtering appropriate candidates for κ-tapering. As an example, Fig. 7 shows the filter curves of meander couplers for the uniform (untapered) case and for κ-tapering by a Blackman window. The side-lobes of the filter are obviously significantly smaller, that is, the crosstalk is substantially reduced.

It should be noted that side-lobe suppression by κ-tapering can be realized only at the expense of an increased device length or coupling coefficient. Typically, a factor of 2 . . . 3 is needed to ensure efficient suppression. The classical window functions (11) such as Hamming, raised cosine, Blackman, and Kaiser windows, are usually preferred since they provide excellent side-lobe suppression.

Uniform Directional Couplers

Figure 8 shows a typical directional coupler consisting of two single-mode waveguides with a longitudinally uniform coupling region and branching regions at both ends of the device.

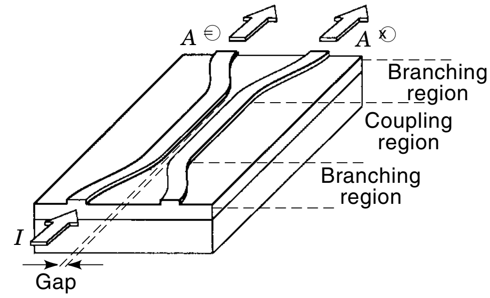

Figure 8. Symmetrical directional coupler composed of rib waveguides. The coupling and branching regions and the gap of the waveguides are identified.

Within the framework of coupled mode theory, the matrix elements of the transfer matrix in Eq. (28), $A^{\ominus}_{+}$ and $A^{\otimes}$, are given by Eq. (32), where L describes the device length, $\delta = k_0\,\Delta n/2$ the detuning of the eigenmodes of the isolated waveguides and $\delta_{\text{eff}} = \sqrt{\delta^2+\kappa^2} = k_0\,\Delta n_c/2$ that of the coupler. If both sets of eigenmodes are available from a numerical analysis, the coupling coefficient κ can be written as $\kappa = \sqrt{\delta_{\text{eff}}^2 - \delta^2}$. The beat length of the uniform coupler is given by $L^{\ominus} = 2\pi/\delta_{\text{eff}}$, its coupling length by $L_{\otimes} = \pi/\delta_{\text{eff}}$.

Symmetrical Coupler. A symmetrical directional coupler maintains the phase mismatch $\delta = 0$ over the full spectral range. Its transfer function has a sinusoidal wavelength characteristic irrespective of the shape of the branching regions (6). A symmetrical coupler which separates two wavelengths λ_1 and λ_2, for example, 1300 nm and 1500 nm, usually has a length equal to one coupling length at λ_1 and two at λ_2. It has a wide passband and a narrow stopband due to its sinusoidal filter characteristic. Symmetrical directional couplers have infinitely many perfect bar and cross states.

Symmetrical couplers have been fabricated as fiber based and integrated optical devices in various material systems, for example, SiO_2/Si, $LiNbO_3$, ion exchange in glass, InGaAsP/InP, and GaAlAs/GaAs. Today, fused fiber couplers are optical filters widely used as broadband filters (e.g., for 1.3/1.5 μm) or taps in communications systems.

Asymmetrical Coupler. An asymmetrical coupler consists of two different waveguides. It has infinitely many perfect bar states $I^{\otimes} = 0$ but usually imperfect cross states. Its filter characteristic is given by $I^{\otimes} = F\,\sin^2(\delta_{\text{eff}}L)$ where the Lorentzian-shaped envelope is

$$F = \frac{\kappa^2}{\kappa^2+\delta^2} \tag{34}$$

To calculate the number of channels which can be separated by an asymmetrical coupler it is useful to consider typical spacings between adjacent channels. Figures of this kind are the full width half maximum $\Delta\lambda_{\text{FWHM}}$ and the spectral distance $\Delta\lambda^{\ominus}$ to the adjacent bar states.

$$\Delta\lambda^{\ominus} = \pi \bigg/ \left(L\frac{\partial\delta}{\partial\lambda}\right) = \lambda\left\{L\left(\frac{\partial\Delta n_{\text{eff}}}{\partial\lambda} - \frac{\Delta n_{\text{eff}}}{\lambda}\right)\right\}^{-1} \tag{35}$$

$$\Delta\lambda_{\text{FWHM}} = \frac{\sqrt{3}}{2}\Delta\lambda^{\ominus} \tag{36}$$

In comparison to a symmetrical directional coupler, the FWHM of an asymmetrical coupler is reduced and the stopband is significantly wider. The width of the passband decreases for increasing device length L, that is, with a decreasing coupling coefficient. Thus the ratio of bandwidth to device length can be used as a measure for the efficiency of an asymmetrical coupler. The maximum power transfer at the cross state is given by $I^{\otimes} = |\kappa/\delta_{\text{eff}}|^2$, that is, the cross state is imperfect as long as the detuning $\delta \neq 0$ does not vanish at the crossover wavelength. Figure 9 shows the filter curve of an asymmetrical directional coupler whose waveguide arms have different material compositions and geometries. Complete crossover is achieved only for specific layouts which guarantee the coincidence of the wave numbers at the design wavelength. A good guideline for the design is to make the product of waveguide cross section and refractive index contrast for both waveguide core regions equal at the design wavelength.

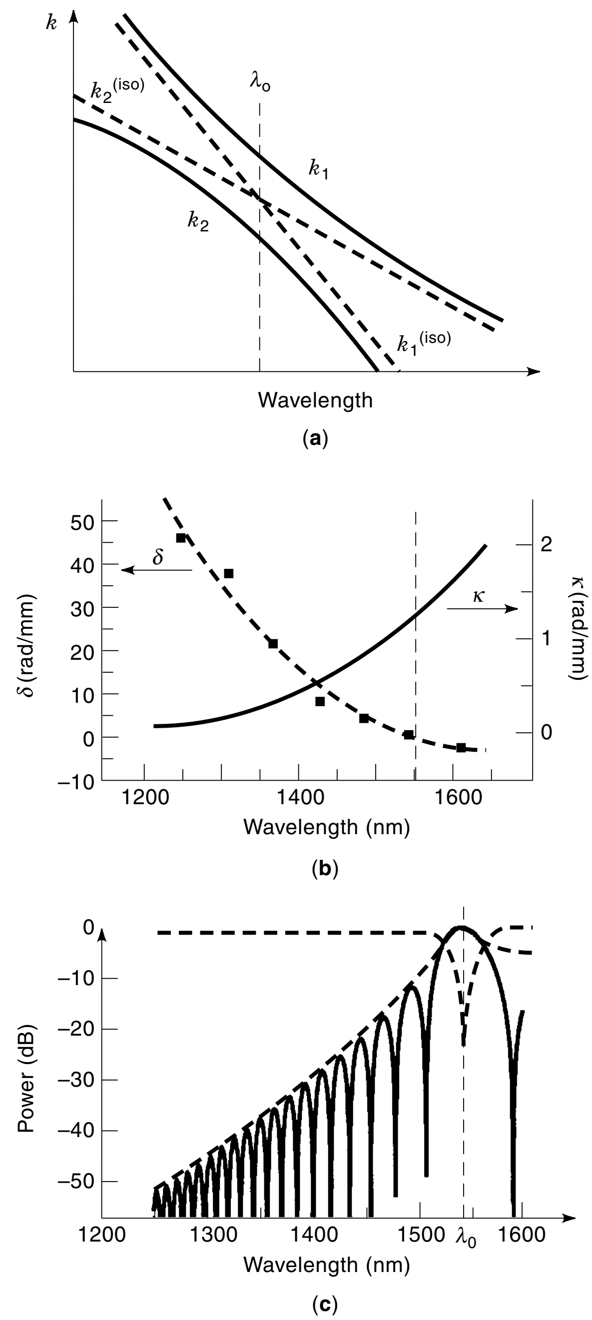

Figure 9. Asymmetrical coupler: (a) eigenmodes for isolated and coupled waveguides, (b) $\delta(\lambda)$ and $\kappa(\lambda)$ from (a), (c) low crosstalk for de/multiplexer at 1550 nm due to asymmetry.

Figure 9(a) shows the crossover of the eigenmodes of the isolated waveguides and the detuning of the coupler modes as a function of the wavelength. This diagram can be used to obtain the required values of the detuning δ and the coupling coefficient κ, as is shown in Fig. 9(b). It should be noted that the two curves are not straight lines as assumed within coupled mode theory. Figure 9(c) shows the dispersion diagram of an asymmetrical coupler. The design of an asymmetrical coupler is restricted to certain waveguide combinations.

Grating Assisted Asymmetrical Couplers

Use of an overlay grating allows the design space of asymmetrical couplers to be enlarged. The ratio of the FWHM to the device length in particular can be significantly reduced by using two waveguides with minimum and maximum refractive index contrasts, each with the maximum core area leading to single-mode operation. Phase matching can be achieved for the design wavelength λ_0 by introducing a period

$$\Lambda = \frac{\pi}{\delta(\lambda_0)} \tag{37}$$

Any periodically varying waveguide structure that changes the waveguide thickness or refractive index can be used. Thickness variations are implemented by etching processes, refractive index variations often by (e.g., electro- or thermooptical) tuning.

A cross section of a grating assisted coupler (meander coupler) is shown in Fig. 6(b). The filter curves are sinc-like functions, as has been shown for the asymmetrical coupler (see Fig. 9). One period of a meander structure based on a rectangular grating of tooth height h_g is described by

$$\mathscr{U}_{\text{unit}} = \mathscr{U}_{\text{CM}}(\delta, \kappa, \Lambda/2) * \mathscr{U}_{\text{CM}}(\delta, -\kappa, \Lambda/2) \tag{38}$$

$$\kappa(\lambda) = \frac{\pi a_{12}(\lambda, h_g)}{\Lambda} \tag{39}$$

The definition of the detuning δ coincides with that of the asymmetrical coupler. The coupling coefficient κ for one section is correlated with the overlap integral a_{12} [Eq. (33)].

The transfer matrix of a uniform grating assisted coupler can be calculated by using Chebyshev polynominals (see Appendix). For a nonuniform grating (chirp, κ-tapering), the filter has to be stacked section by section.

Figure 10 shows the experimental and theoretical results for a κ-tapered meander coupler in InGaAsP/InP with a period of $\approx$100 μm. The coupler is built up from curved waveguides to reduce the radiation losses. Since both waveguide arms forming the coupler have the same material composition, the full width half maximum was 40 nm. By using different material compositions, this figure can be reduced to only 1 nm for a 10-mm long device.

To overcome the limitations of a fixed grating structure, an electrode and a control scheme can be used to synthesize each grating period individually. The basic idea of the Syngrat layout is to use four independently controlled electrodes for each period (12). A tuning range from λ =1250 nm to 1600 nm with a channel separation of 1 nm can be realized with the expenditure of several thousand electrodes. The use of tuned gratings allows the filter to be reconfigured dynamically. Moreover, the wavelength channels can be addressed directly after a scaling procedure.

The Syngrat is a forward transverse filter. It can be used to add or drop a set of wavelengths in a single step by super-

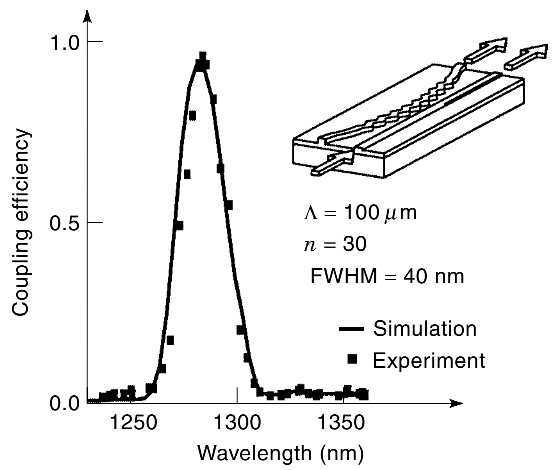

Figure 10. Experimental and theoretical filter curves for a κ-tapered meander coupler in InGaAsP/InP (30 periods with a length of each 100 μm, 2 . . . 5 μm waveguide separation).

position of the set of required gratings. This is done by summing all the individual coupling coefficients. This concept would enlarge the design space and the flexibility for add/drop filters in WDM systems (7).

Mach–Zehnder Devices

Mach–Zehnder devices represent compound components consisting of a phase shifter embedded between two Y-branches or directional couplers. The 4-port Mach–Zehnder coupler can be used as an optical filter or switch. The operation of a properly designed Mach–Zehnder device is mainly driven by the phase shifter. Its transfer matrix is given by

$$\overline{\mathscr{U}} = \begin{pmatrix} \cos\phi_1 & j\sin\phi_1 \\ j\sin\phi_1 & \cos\phi_1 \end{pmatrix} \begin{pmatrix} e^{j\Delta\varphi/2} & 0 \\ 0 & e^{-j\Delta\varphi/2} \end{pmatrix} \begin{pmatrix} \cos\phi_2 & j\sin\phi_2 \\ j\sin\phi_2 & \cos\phi_2 \end{pmatrix} \tag{40}$$

with the phase thicknesses ϕ_1 and ϕ_2 of the two couplers and the relative phase shift $\Delta\varphi$ of the phase shifter.

The directional couplers within the Mach–Zehnder chain are constructed as follows. Each coupler has a phase thickness ϕ_i, the overall phase thickness being $\pi/2$. In the uniform case, all couplers are identical. Analogously to the grating assisted couplers, the coupling coefficients can be tapered, resulting in reduced crosstalk. Figure 11 shows calculated filter curves of a chain of ten Mach–Zehnder couplers for the uniform case and two tapered ones. It should be noted that the filter curves look similar to those of asymmetrical couplers.

For a required crosstalk attenuation of 20-dB, a 10-stage filter with a Blackman window can be used to separate only three wavelength channels.

Bragg Gratings

Bragg gratings, that is, single-mode slab or stripe waveguides or single-mode fibers equipped with an appropriate periodic overlay, represent the most elementary and at the same time

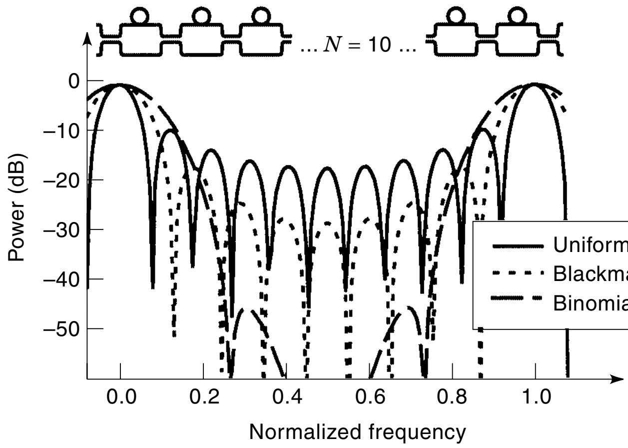

Figure 11. Filter curves for a chain of ten Mach–Zehnder interferometers for the uniform and κ-tapered cases.

most important example of contradirectionally coupled devices in guided wave optics. The Bragg condition

$$\Lambda = \frac{\lambda_0}{2n} \tag{41}$$

determines the spectral position of the stopband.

The elements of the transfer matrix Eq. (28), $A^{\ominus}$ and $A^{\otimes}$, calculated within the framework of coupled mode theory are given by Eq. (32), where L describes the device length, $\delta = k_0\,\Delta n/2 - \pi/\Lambda$ the detuning of the eigenmodes of the isolated waveguides under the influence of the Bragg grating and $\delta_{\text{eff}} = \sqrt{\delta^2 - |\kappa|^2}$ the effective detuning. κ describes the Fourier coefficient responsible for the contradirectional coupling. For a rectangular grating, it is given by $\kappa = \Delta n/(\Lambda\bar{n})$. The reflectance of the Bragg grating is given by

$$R = \frac{|\kappa|^2 \sin^2(\delta_{\text{eff}}L)}{\delta_{\text{eff}}^2 \cos^2(\delta_{\text{eff}}L) + \delta^2 \sin^2(\delta_{\text{eff}}L)} \tag{42}$$

and its transmittance by $T = 1 - R$. In contrast to the corresponding codirectional coupler, the effective detuning of a (lossless) Bragg grating can become purely imaginary if $\delta^2 < |\kappa|^2$. Figure 12 shows the increasing reflectance within the stopband for increasing values of κL.

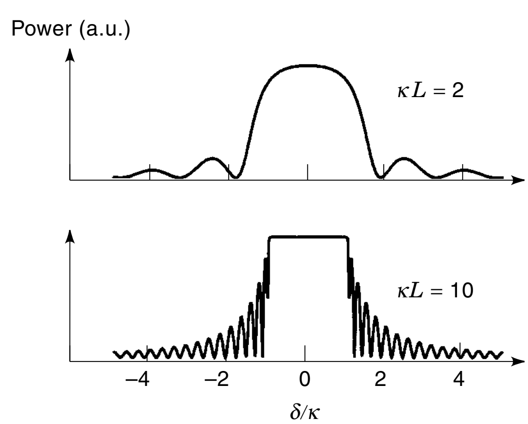

Figure 12. Filter curves for uniform Bragg gratings with $\kappa L = 2$ (a), $\kappa L = 10$ (b).

Bragg gratings exhibit radiation on the short-wave side of the fundamental Bragg peak (13), the efficiency of the coupling depending on the layout of the grating (geometry and refractive indices). When operated at oblique incidence, these gratings show polarization conversion and a Brewster angle for TE polarization (14).

Bragg gratings can be stacked together in order to realize compound devices. For example, by putting a $\lambda/4$ spacer between two identical gratings of this kind, it is possible to realize an extremely narrow passband in the center of the stopband of the original gratings (see Fig. 5 for a typical filter curve). In the same way, it is possible to derive the filter curve for any type of chirped and tapered Bragg gratings.

Chirped Bragg gratings are promising candidates for disperion-compensating filters. Because of the chirp, the effective reflection point, that is, the group delay, shifts rapidly if the wavelength is varied. It should be noted that the chirp must be controlled perfectly in order to avoid ripples in the dispersion curves.

Bragg gratings designed as optical filters have been realized in fibers and as integrated optical devices in the SiO_2/Si and InGaAsP/InP material systems. The grating structures with periods of ≈ 1 μm for fibers and the SiO_2/Si material system and <0.5 μm for the InGaAsP/InP material system, are implemented by holography or by using phase masks.

Fiber Bragg gratings are commercially available today. They are used as optical filters for communications systems operating in the wavelength division multiplex mode (WDM) or as dispersion compensating filters. Fiber Bragg gratings incorporated in the phase shifter of a Mach–Zehnder coupler are used as ADD/DROP devices.

DIFFRACTION GRATINGS AND OPTICAL PHASED ARRAYS

Spectrographs are based on the interference of multiple beams which are fed from the input signal. The beams interfere in a free-space or a slab waveguide region. Focusing spectrographs provide both diffraction and imaging within a single device.

Theory

For the sake of simplicity the theoretical treatment of focusing spectrographs is restricted here to planar devices. The extension to three dimensions is straightforward (15).

Light-Path Function. The treatment of spectrographs based on the light-path function represents a generalization of Huygen's principle for tackling focusing gratings. The light-path function

$$F(y) = F_I(y) + \overline{PD} - \overline{OD} + m\lambda G(y) \tag{43}$$

describes the effective path difference between a ray propagating from the point of incidence I to the observation point $D = (y_D, z_D)$ via an intermediate point $P = (y, z_G(y))$ at the grating line $z_G(y)$ and the central ray of the beam propagating

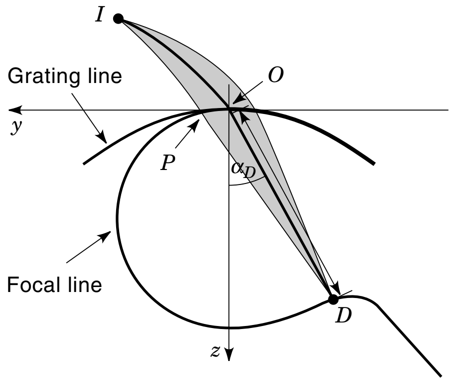

Figure 13. Coordinate system for the analysis of a planar spectrograph.

via the center $O = (0, 0)$ of the grating line (see Fig. 13). The coordinate system is oriented such that the grating line $z_G(0)$ is tangential to its y-axis. The first term $F_I(y) = \widetilde{IP} - \widetilde{IO}$ stands for the effective path difference of the fan-in region, this contribution. It varies for different types of spectrograph. The next two terms on the right-hand side of Eq. (43) account for the physical path difference between the emergent rays. The last term, $m\lambda G(y)$, describes the contributions of the (almost) periodic structure of the grating to the effective path difference operated in the mth diffraction order. For further analysis, the light-path function $F(y)$ is expanded into a rapidly converging Taylor series.

Stigmatic Points. A focusing grating forms a perfect, that is, completely aberration-free, image of the incoming beam if the light-path function $F(y) \equiv 0$ vanishes along the entire grating line. This rigid condition can be satisfied for only a few points in the observation plane at best. Such aberration-free observation points are designated as stigmatic points of the mounting.

Imaging. If only the leading coefficients of the Taylor expansion of the light-path function vanish, images exhibiting aberrations will occur. By determining the observation point in the slab waveguide, it is usually possible to make the first two expansion coefficients vanish.

Fermat's principle ($F'(0) = 0$) yields the diffraction angle α_D via the grating equation

$$\sin\alpha_D = -F_I'(0) - m\lambda G'(0) \tag{44}$$

The image, that is, the waist of the diffracted beam, is located at a distance

$$r_D = \frac{\cos^2\alpha_D}{-m\lambda G''(0) - F_I''(0) + z_G''(0)\cos\alpha_D} \tag{45}$$

away from the center O of the grating line. The focal line $\mathbf{r}_f$, that is, the image curve of the grating, is then given by

$$\mathbf{r}_f = r_D \begin{pmatrix} -\sin\alpha_D \\ \cos\alpha_D \end{pmatrix} \tag{46}$$

It should be noted that spectrographs will not always form a real image. In particular, gratings will often not form an image at all.

Magnification. The ratio of the spot magnifications m_D and m_E of two arbitrarily chosen observation points D and E is given by

$$\frac{m_D}{m_E} = \frac{r_D\cos\alpha_E}{r_E\cos\alpha_D} \tag{47}$$

The contours of constant spot magnification are formed by a family of circles which are tangential to the grating line at its center O.

Rowland Mountings. A Rowland-type mounting is an unchirped spectrograph ($G^{(\nu)}(0) = 0,\ \nu > 1$). Its grating line $z_G(y) = R - \sqrt{r^2 - y^2}$ is a semicircle of radius R. The point of incidence is chosen such that the phase portrait along the grating line becomes linear ($F_I^{(\nu)}(0) = 0,\ \nu > 1$).

The focal line of a Rowland-type mounting is given by a circle of radius $r = R/2$ that is tangential to the grating line at its center O. Rowland-type mountings offer constant spot magnification and low aberrations.

Aberrations. Further expansion coefficients $F^{(\nu)}(0)$ with $\nu > 2$ can be made to vanish only for special mountings. They represent the aberrations of the spectrograph. The leading term $F'''(0)$ designates the coma, and the following contribution $F^{(\mathrm{IV})}(0)$ the spherical aberration. Astigmatism represents the most significant aberration for three-dimensional spectrographs. It cannot occur in planar devices. In order to obtain the maximum spectral resolution, designs usually aim to minimize the aberrations of the grating. As a rule of thumb, a focusing spectrograph will form a good image as long as the path difference between the central and $1/e$ ray is smaller than a tenth of the wavelength ($F(y_{1/e}) < \lambda/10$). It should be noted that it is impossible to design a planar spectrograph which exhibits neither coma nor spherical aberration over an extended spectral range. Only Rowland-type mountings have no coma.

Efficiency. The shape of a single diffraction peak represents the Fourier transform of the envelope of the optical field emitted from the grating line. The Fourier transform of the near-field of a single grating groove forms the envelope of the diffraction pattern (see Fig. 14). For curved gratings, the central rays emitted from all partial beams must intersect each other at a single point which can be regarded as the "blaze point" of the mounting. This point should obviously be located on the focal line.

A few remarks on the electromagnetic theory of reflection gratings are relevant here. Since the boundary conditions at the corrugated surface of a grating differ for the different vector components of the electric and magnetic fields, the efficiency curves of the reflection gratings will be affected by the vectorial character of the incoming beam. In consequence, the envelope of the diffraction pattern of a reflection grating will always exhibit polarization-dependent behavior. The theory of plane reflection gratings for optical instruments is extensively examined in a book edited by Petit (16). The efficiency curves of such gratings exhibit a rich variety of physical effects in-

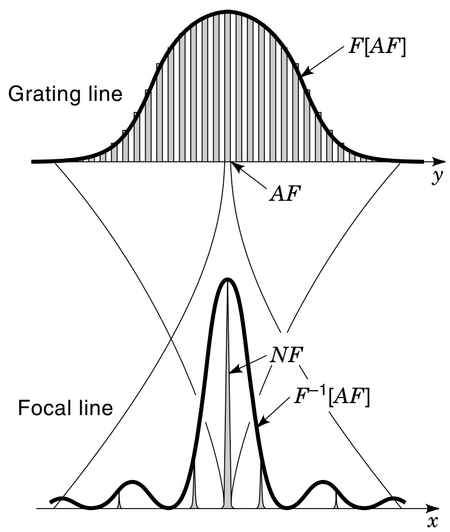

Figure 14. Diffraction efficiency of spectrographs.

cluding Wood anomalies and the excitation of surface waves (surface plasmons).

Spectral Resolution and Free Spectral Range. The spectral resolution of a spectrograph is governed by the number of illuminated grating grooves. According to Rayleigh's criterion, it is given by [see Eq. (10)]

$$d\lambda_{\mathrm{RC}} = \frac{\lambda}{|m|N} \tag{48}$$

The spectral resolution required for practical devices (see (6), Ch. 9) depends on the underlying application, essentially on the specified crosstalk attenuation between adjacent wavelength channels.

The maximum diffraction order is determined by the required free spectral range. The period $\Lambda_m = |m|\Lambda_1$ of an mth-order spectrograph represents a multiple of the period of the equivalent first-order device, that is, the fabrication of spectrographs can be simplified at the expense of a reduced spectral range. In fact, planar spectrographs used in optical communications systems often exhibit the maximum diffraction order that is permitted, and devices with $|m| > 100$ have been realized. The number of accessible wavelength channels N_{ch} is given by the quotient of free spectral range and spectral resolution.

Reflection and Transmission Gratings

The physical path difference for the fan-in region of a grating is given by $F_I(y) = \overline{IP} - \overline{IO}$, where I represents the point of incidence and P an arbitrary point on the grating line. Its derivatives at the center O of the grating line are given by $F_I'(0) = \sin\alpha_I$ and $F_I''(0) = \cos^2\alpha_I/r_I - z_G''(0)\cos\alpha_I$. The spot magnification factor is given by $m_0 = (r_D\cos\alpha_I)/(r_I\cos\alpha_D)$, where α_D designates the diffraction angle and r_D the distance between the center of the grating line and the image D. The parameters α_I and r_I describe the corresponding parameters of the input beam. Gratings are blazed by orienting the grating grooves such that all reflected rays intersect at the blaze point, which may be located at infinity for nonfocusing devices.

Transmission Gratings. Transmission gratings are divided into amplitude and phase gratings. Amplitude gratings modulate the amplitude distribution along the phase front by a series of (usually equidistant) slits. They represent the most classical type of grating dating back to Fraunhofer. Due to the excess loss (usually 3 dB), they are of minor technical interest today. Phase gratings, in contrast, modify the phase portrait without changing the amplitude distribution. They are much more attractive but hard to fabricate.

Integrated optical transmission gratings have been realized by several groups. Up to now, none of these devices has entered the market.

Reflection Gratings. A focusing reflection grating is a more compact solution since it represents a folded optical system. The classical Rowland mounting is based on a reflection grating.

Most reflection gratings manufactured today represent replicas of ruled master devices. Such gratings are preferred due to their high efficiency. However, marginal mechanical imperfections of the ruling machines result in aberrations of the grating. In particular, periodic perturbations yield "ghosts" of the grating, that is, in satellite peaks within their spectra. Holographic exposure makes it possible to fabricate gratings which do not exhibit any ghosts, although at the expense of a significantly reduced efficiency. Holographic gratings allow for stigmatic points, but the impacts of the holographic setups limit this feature to a few types of mounting (17).

Planar spectrographs based on reflection gratings have also been successfully fabricated. The reflection gratings were realized by etching into a slab waveguide or by processing the chip endface. The technologies of integrated optics allow, in contrast to those for classical spectrographs, the gratings to have an arbitrary shape and chirp. This increased flexibility is counterbalanced by restrictions on geometry and chip area which are characteristic of integrated optics. Integrated optical gratings have been realized by several groups. Figure 15 shows a flat-field spectrograph. The point of incidence and the focal line of this device are located at the chip endface. Integrated optical reflection gratings are currently available on the market.

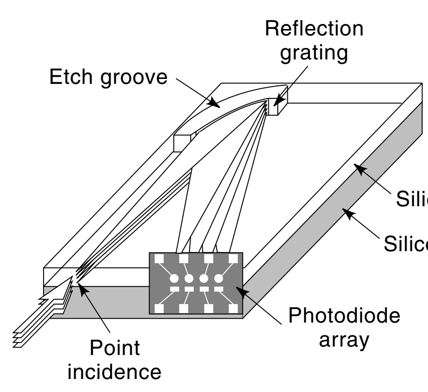

Figure 15. Integrated optical flat-field spectrograph in the silica-on-silicon (SiO_2/Si) material system.

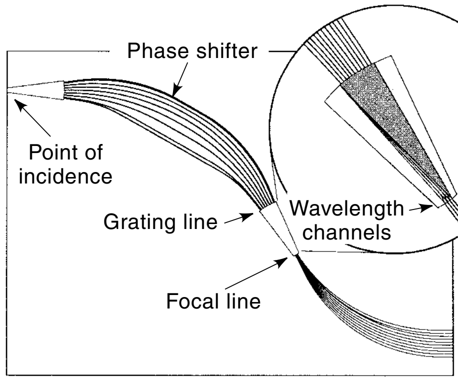

Figure 16. Optical phased array chip: principle of operation.

Optical Phased Arrays

An optical phased array—also called an arrayed waveguide grating (AWG) or a phasor—represents a phased transmission grating (6,18). In contrast to more conventional devices of this kind, it allows a huge phase shift and thus operation at extremely high diffraction orders.

Figure 16 shows a schematic drawing of a optical phased array. The point of incidence I of the phased array is located at the beginning of the left slab waveguide. Starting from this point, the input beam propagates under the influence of diffraction through the homogeneous slab waveguide. At the front end of the phase shifter, the optical far-field represents the Fourier transform of the near-field of the input beam. The beam is then divided into N partial beams, each propagating separately through one of the strip waveguides forming the phase shifter. The phase shifter allows the phase positions of the partial beams to be individually adjusted relative to each other, that is, the phase portrait at the grating line, which is located at the input side of the second slab waveguide, to be tuned. The endfaces of the strip waveguides forming the grating line replace the grating grooves of a conventional grating. If the front and back of the phase shifter have the same layout, the optical field at the grating line will represent the Fourier transform of the near-field at the input side modified by the phase portrait due to the phase shifter. The near-field at the point of incidence will be reconstructed at the focal curve provided the optical system of the phased array does not exhibit any aberrations.

The period of the phased array is given by the spacing of the strip waveguides at the back of the phase shifter (projected to the tangent at the center of the grating line). In order to prevent coupling between the strip waveguides forming the phase shifter, practical designs tend to be based on the maximum diffraction order allowed by the free spectral range of the underlying application. The blazing of phased arrays is straightforward. The axes of the waveguides ending at the grating line should intersect the focal curve at a common point, which is the blaze point of the device.

For a phased array, the light-path difference between the point of incidence I and the grating line $z_G(y)$ is given by $F_I(y) = \overline{IP_I} - \overline{IO_I} + (n_p/n_s)(\widetilde{P_IP} - \widetilde{O_IO})$ where O represents the center of the grating line and P an arbitrary point on it. The other two points O_I and P_I are located on the input side of the phase shifter. They are connected with their counterparts O and P by the strip waveguides of the phase shifter. The tilde on top of $\widetilde{P_IP}$ and $\widetilde{O_IO}$ designates the arc length along the corresponding strip waveguides. The ratio n_p/n_s accounts for the phase difference caused by the different effective propagation constants of the strip n_p and slab n_s waveguides. The front side of the phase shifter usually represents a circle whose center is located at the point of incidence. The first two terms $(\overline{IP_I} - \overline{IO_I})$ will therefore often compensate each other.

The Rowland mounting represents the most popular layout for optical phased arrays. The groove function for such devices is given by $G(y) = y/\Lambda$ where Λ designates the period of the optical phased array (projected onto the tangential coordinate axis y). The grating line is given by a semicircle of radius R. The fan-in of the phased array must be assembled such that the phase portrait becomes linear along the grating line. The light-path difference on the input side is then given by

$$F_I(y) = \left(-m\frac{\lambda_C}{\Lambda} - \sin\alpha_C\right)y = \frac{n_p\Delta L}{n_s\Lambda} \tag{49}$$

in which λ_C designates a design wavelength (inside the slab waveguide), α_C the diffraction angle for this wavelength and Δ_L the path difference between two adjacent waveguides. As pointed out earlier, planar Rowland mountings exhibit no coma. The Rowland mounting which forms the basis for the optical phased array is operated close to the vertex of the Rowland circle ($\alpha_D = 0$), where it exhibits a stigmatic point. Figure 17 shows a set of filter curves for a phased array in the silica-on-silicon (SiO_2/Si) material system. At the expense of an additional insertion loss, the passband of the phased arrays can be flattened by modifying the phase shifter or the waveguides at the point of incidence I or the focal line.

Integrated optical phased arrays are key components within fiber optical transmission systems and networks operated in the wavelength division multiplex mode (WDM). They are used as wavelength demultiplexers separating all wavelength channels in a single step. For transmission systems with many wavelength channels they are also operated as multiplexers in order to avoid the excess loss of wavelength-independent combiners.

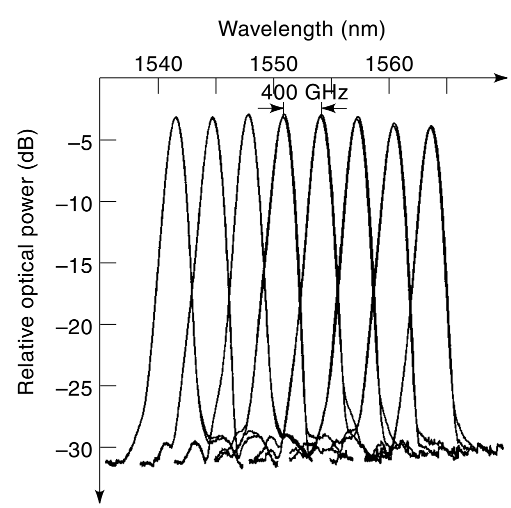

Figure 17. Filter curves of an 8-channel optical phased array in the silica-on-silicon (SiO_2/Si) material system (channel spacing: 400 GHz, TE, and TM polarization).

Optical phased arrays realized in the silica-on-silicon (SiO_2/Si) material system are available on the market, devices in other material systems (InGaAsP/InP, ion exchange in glass, polymers) have been successfully demonstrated. The usability of optical phased arrays in advanced networks containing optical ADD/DROP multiplexers (OADMs) and/or optical cross connects (OXCs) could be verified within a series of field trials.

APPENDIX

Unimodular matrices form a typical mathematical formulation for lossless devices or systems. The characteristic matrices (see section entitled "Interference Filters and Fabry–Perot Interferometers") and transfer matrices (see section entitled "Co- and Contradirectional Couplers") occurring within this article represent typical examples.

A unimodular matrix is any matrix with $\det\mathscr{U} = 1$. Unimodular matrices form a group, that is, the product of two unimodular matrices results in another unimodular matrix. The inverse of a unimodular 2×2 matrix is given by

$$\begin{pmatrix} u_{11} & u_{12} \\ u_{21} & u_{22} \end{pmatrix}^{-1} = \begin{pmatrix} u_{22} & -u_{12} \\ -u_{21} & u_{11} \end{pmatrix} \tag{50}$$

and the eigenvalues are

$$\mu_{1/2} = \mathrm{Tr}\mathscr{U}/2 \pm \sqrt{(\mathrm{Tr}\mathscr{U}/2)^2 - 1} \tag{51}$$

The characteristic matrix of an N-period matrix is given by

$$\mathscr{U}^N = U_{N-1}\left(\frac{\mathrm{Tr}\mathscr{U}}{2}\right)\mathscr{U} - U_{N-2}\left(\frac{\mathrm{Tr}\mathscr{U}}{2}\right)\mathscr{E} \tag{52}$$

where $\mathscr{E}$ is the unity matrix. $U_n(x)$ designates the Chebyshev polynominals of the second kind, that is,

$$U_N(\cos\theta = \sin[(N+1)\theta]/\sin\theta \tag{53}$$

BIBLIOGRAPHY

1. J. E. Greivenkamp, Interference. In M. Bass, E. W. van Stryland, D. R. Williams and W. L. Wolfe (eds.), *Handbook of Optics,* 2nd ed., New York: McGraw-Hill, 1995.
2. A. Yariv and P. Yeh, *Optical Waves in Crystals,* New York: Wiley, 1983.
3. H. A. Macleod, *Thin-Film Optical Filters,* 2nd ed., Bristol: Hilger, 1986.
4. J. A. Dobrowolski, Optical properties of films and coatings. In M. Bass, E. W. van Stryland, D. R. Williams, and W. L. Wolfe (eds.), *Handbook of Optics,* 2nd ed., New York: MacGraw-Hill, 1995.
5. A. Thelen, *Design of Optical Interference Coatings,* New York: McGraw-Hill, 1989.
6. R. März, *Integrated Optics: Design and Modeling,* Boston: Artech, 1994.
7. M. Grawert and H.-P. Nolting, A comparison between different methods to calculate grating assisted asymmetrical couplers, *Linear Nonlinear Integrated Optics, Proc. Europto Series,* **2212**: 328–336, 1994.
8. J. Chilwell and I. Hodgkinson, Thin-film field-transfer matrix theory of planar multilayer waveguides and reflection from prism-loaded waveguides, *J. Opt. Soc. Amer.,* **A1**: 742–753, 1984.
9. P. C. Cross and R. C. Alferness, Filter characteristic of codirectional coupled waveguides with weighted coupling, *IEEE J. Quantum Electron.,* **14**: 843–847, 1978.
10. H. Kogelnik, Filter response of nonuniform almost-periodic structures, *Bell Syst. Tech. J.,* **55**: 632–637, 1976.
11. A. Papoulis, *Systems and Transforms with Application in Optics,* New York: McGraw-Hill, 1968.
12. M. Grawert and H.-P. Nolting, Syngrat, an electro-optically controlled tunable filter with a synthesized grating structure, *Opt. Quantum Electron.,* **27**: 887–896, 1995.
13. K. Furuya, Y. Suematsu, and S. Shigeo, Integrated optical branching filter consisting of three-dimensional waveguide and its nonradiative condition, *IEEE Trans. Circuits Syst.,* **26**: 1049–1054, 1979.
14. K. Wagatsuma, H. Sakaki, and S. Saito, Mode conversion and optical filtering of obliquely incident waves in corrugated waveguide filters, *IEEE J. Quantum Electron.,* **15**: 632–637, 1979.
15. H. Noda, T. Namioka, and M. Seya, Geometric theory of the grating, *J. Opt. Soc. Amer.,* **64**: 1031–1042, 1974.
16. R. Petit (ed.), *Electromagnetic Theory of Gratings,* Berlin: Springer-Verlag, 1980.
17. M. C. Hutley, *Diffraction Gratings,* London: Academic Press, 1982.
18. C. Dragone, Optimum design of a planar array of tapered waveguides, *J. Opt. Soc. Amer.,* **A7**: 2081–2093, 1990.

Reading List

G. P. Agraval, *Fiber-Optic Communication Systems,* 2nd ed., New York: Wiley, 1997.

M. Born and E. Wolf, *Principles of Optics,* 3rd ed., Oxford: Pergamon, 1965.

R. L. Cruz et al., Optical networks, Special issue in *IEEE Sel. Areas Commun.,* **14/5**, 1996.

A. Erhardt et al., Semiconductor laser amplifier as optical switching gate, *IEEE J. Lightwave Technol.,* **11**: 1287–1295, 1993.

M. Fujimura et al. (eds.), Multiwave-length optical technology and networks, Special issue in *IEEE J. Lightwave Technol.,* **14/6**, 1996.

T. K. Gaylord and M. G. Moharam, Analysis and application of optical diffraction gratings, *Proc. IEEE,* **73**: 894–937, 1985.

A. Hardy and W. Streifer, Coupled mode theory of parallel waveguides, *IEEE J. Lightwave Technol.,* **3**: 1135–1146, 1985.

H. A. Haus, *Waves and Fields in Optoelectronics,* Englewood Cliffs, NJ: Prentice-Hall, 1984.

K. O. Hill et al., Photosensitivity in optical fibers, *Annu. Rev. Mater. Sci.,* **23**: 125–157, 1993.

R. Kashyap et al., Light-sensitive optical fibers and planar waveguides, *British Telecom Technol. J.,* **11**: 150–160, 1993.

M. Kawachi, Planar lightwave circuits for optical FDM, *Proc. OEC'92,* 302–303 (1996).

H. Kogelnik, Coupled wave theory for thick hologram gratings, *Bell Syst. Technol.,* **48**: 2909–2947, 1969.

W. H. Louisell, *Coupled Mode and Parametric Electronics,* New York: Wiley, 1960.

H. Nishihara, M. Haruna, and T. Suhara, *Optical Integrated Circuits,* New York: McGraw-Hill, 1989.

G. W. Stroke, Diffraction gratings, in S. Flügge (ed.), *Encyclopedia of Physics,* **24**, *Optical Instruments,* Berlin: Springer, 1967.

A. Yariv, Coupled mode theory of guided wave optics, *IEEE J. Quantum Electron.,* **9**: 919–933, 1973.

HANS-PETER NOLTING
Heinrich-Hertz Institut
REINHARD MÄRZ
Siemens AG

OPTICAL FILTERS. See ELECTRO-OPTICAL FILTERS.

OPTICAL FREQUENCY CONVERSION. See OPTICAL HARMONIC GENERATION PARAMETRIC DEVICES.